Chapter 34

Soft X-ray Spectromicroscopy of Protein Interactions with Phase-Segregated Polymer Surfaces

Adam P. Hitchcock,[*,a] Bonnie O. Leung,[b] John L. Brash,[c] Andreas Scholl,[d] and Andrew Doran[d]

[a]Chemistry and Chemical Biology, BIMR, McMaster University, Hamilton, Ontario, Canada L8S 4M1
[b]Alberta Environment and Sustainable Resource Development, Edmonton, Alberta, Canada T5K 2J6
[c]School of Biomedical Engineering, McMaster University, Hamilton, Ontario, Canada L8S 4M1
[d]Advanced Light Source, Berkeley Lab, Berkeley, California 94720, U.S.A.
[*]E-mail: aph@mcmaster.ca

Quantitative spectro-microscopic characterization of the interfaces between polymers and relevant proteins helps understand fundamental issues of protein – polymer interactions and can provide insights into biocompatibility. Synchrotron based X-ray photoemission electron microscopy (X-PEEM) and scanning transmission X-ray microscopy (STXM) are being used to study distributions of proteins adsorbed on chemically heterogeneous polymer surfaces with ~30 nm spatial resolution. The relevant contrast in each technique is X-ray absorption spectroscopy which provides speciation and quantitation of both adsorbed proteins or peptides (and in combinations), simultaneously with chemically sensitive imaging of the underlying polymer substrate. An overview of recent progress in this field is given, along with some comparisons to complementary techniques (AFM and TOF-SIMS) for investigating protein-polymer interfaces.

In Proteins at Interfaces III State of the Art; Horbett, T., et al.;
ACS Symposium Series; American Chemical Society: Washington, DC, 2012.

Keywords: photoemission electron microscopy; X-PEEM; scanning transmission X-ray microscopy; STXM; NEXAFS; AFM; TOF-SIMS; mapping; protein adsorption; HSA; polystyrene; poly(methyl methacrylate)-b-polyacrylic acid; blend

Introduction

Understanding and controlling protein interactions with surfaces are important aspects of biomaterials optimization for medical applications. Polymers are often used in medical technology. Typically the polymers chosen are ones whose surface chemistry and morphology are optimal for specific medical applications, either in their pure form or with suitable surface coatings (*1*). The nature and spatial arrangements of surface chemical motifs can lead to a biocompatible surface, or lead to adverse interactions, ultimately triggering the foreign body response (*2*), thrombus formation etc. In general, proteins are the first species to adsorb to biomaterials and thus much of biomaterials optimization involves controlling protein surface interactions. In this context control may refer to complete prevention or minimization of adsorption (protein resistance, antifouling) or it may refer to the selective promotion of adsorption of one specific protein relative to all others from the complex mix of species present in the biological tissue or fluid with which the biomaterial is in contact.

Reduction or elimination of protein adsorption is often the goal for medical devices, while controlled protein adsorption may be important for biochemical sensors (*3*, *4*) and nanofluidic systems (*5*). Reduction of protein adsorption or controlled adsorption of proteins may be possible by exploiting electrostatic interactions. For instance, nanopatterning of carboxyl-terminated self assembled monolayers (SAMs) with lysozyme for biosensor applications gives protein patterns based on the interaction of the positively charged protein with the negatively charged surface (*6*). Repulsive electrostatic interactions can reduce protein adsorption (*7*) but cannot prevent it entirely (*8*). Other major driving forces for protein adsorption include hydrogen bonding, van der Waals forces, and hydrophobic interactions (*9*).

For the past decade we have been systematically exploring the use of synchrotron based soft X-ray spectromicroscopy to study the surface chemistry of polymeric biomaterials and their interactions with relevant proteins and peptides. Most of our work in this area has involved development and exploitation of X-ray photoemission electron microscopy (X-PEEM), although a number of studies have also been carried out using scanning transmission X-ray microscopy (STXM). A comprehensive review of X-PEEM research on biomaterials up to 2009 was recently published (*10*) while recent reviews of the field of soft X-ray microscopy (*11–13*) place these studies in a broader context. In this chapter, we describe the X-PEEM and STXM techniques as applied to studies of proteins at interfaces. We compare the advantages and limitations of each technique, in some cases relative to other frequently used protein-polymer interface probes

such as atomic force microscopy (AFM) and time-of-flight secondary ion mass spectrometry (TOF-SIMS). We illustrate the capabilities of these techniques by summarizing selected recent studies including:

- the effect of pH on adsorption of human serum albumin (HSA) and a cationic antimicrobial peptide, RWWKIWVIRWWR-NH_2 (sub-6) to the surface of a phase segregated blend of polystyrene (PS) and a copolymer, poly(methyl methacrylate)-b-polyacrylic acid (PMMA-PAA) (X-PEEM) (*14*)
- the effect of buffer on the adsorption of HSA to the surface of a phase segregated blend of PS and polylactide (PLA) (X-PEEM) (*15*)
- The effect of an aqueous environment on the adsorption of HSA to the surface of a phase segregated blend of PS/PMMA (X-PEEM, STXM) (*16*)
- the selective adsorption of fibrinogen (Fg) to the interfaces of styrene-b-acrylonitrile (SAN) and the polyether-rich matrix of a complex multi-component reinforced polyurethane (*17*). In this study the interface adsorption was measured in the presence of the protein solution (STXM)
- adsorption of Ac-LKKLLKLLKKLLKL-OH, a model α-helix peptide, on to a patterned micro-array of alcohol and carboxylate terminated self-assembled monolayers (SAM) (X-PEEM, TOF-SIMS)
- adsorption of ubiquitin on plasma polymerized polymers patterned using e-beam lithography (X-PEEM) (*18*)

Soft X-ray Spectromicroscopy Methods

X-PEEM Applied to Protein–Polymer Interactions

Photoemission electron microscopy (PEEM) is a full field technique which provides a magnified image of an illuminated area, derived from the lateral spatial distribution of electrons emitted from the surface. PEEM can be performed using a variety of photoionization light sources, from laser or Hg lamp illumination in laboratory implementations, where topography and work function contrast dominate, to synchrotron X-ray illumination (X-PEEM), where chemical (from NEXAFS or photoemission) and magnetic (from X-ray magnetic circular dichroism) contrast are additional contrast mechanisms. Figure 1 presents a schematic of the X-ray optics (Figure 1a) and electron microscope (Figure 1b) components of the PEEM-2 instrument (*19*) at the Advanced Light Source (ALS), where most of our measurements have been performed. Samples are typically a thin (< 100 nm, to avoid charging) polymeric layer on a Si wafer, which has been exposed to a protein or peptide solution under a well defined regime, thoroughly rinsed prior to drying to remove non-adhering protein, and introduced into the ultrahigh vacuum of the X-PEEM via a load-lock.

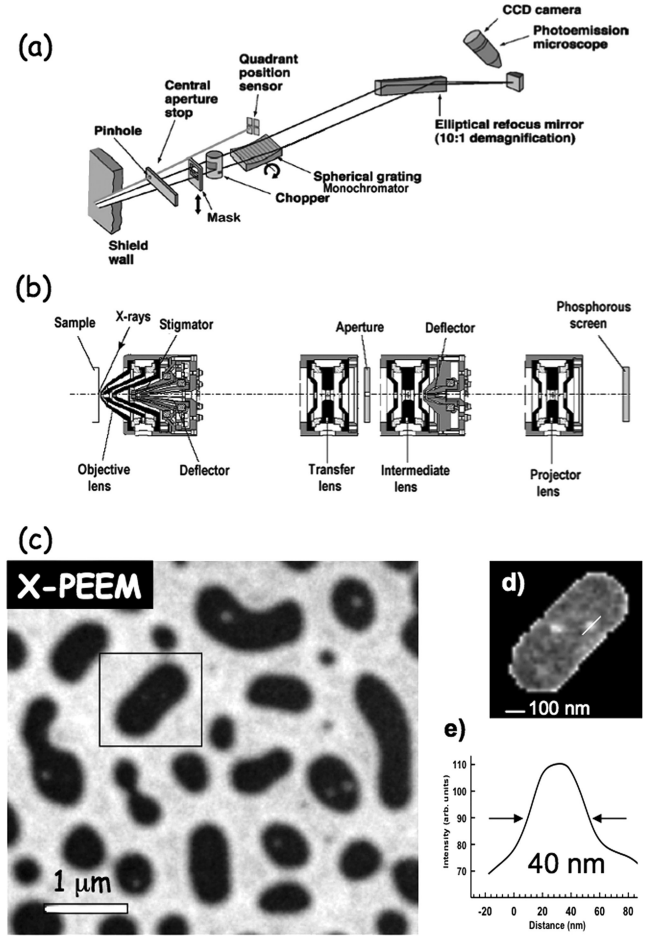

Figure 1. a) Layout of the 7.3.1 bend magnet beam line at the Advanced Light Source (ALS, Berkeley, CA) (19) where most of the X-ray photoemission electron microscope (X-PEEM) results presented in this chapter were obtained. b) schematic of the PEEM-2 microscope (19). c) Image recorded with the ALS PEEM-3 (without the aberration corrector) of a polystyrene - polymethyl-methacrylate (PS/PMMA) (30/70) blend sample, using a photon energy of 285.15 eV, the C 1s →π peak of PS. The logarithm of the intensity is presented to visualize the PS microdomains present in the PMMA macrodomains. d) expanded image of the single PMMA domain indicated in (a). e) line profile across the PS microdomain indicating a flat topped character of the 40 nm wide microdomain. The effective spatial resolution is estimated from the edge sharpness to be 30 nm.*

Figure 1 also presents images from the recently developed PEEM-3 instrument (*20*) on ALS beamline 11.0.1, which has somewhat superior spatial resolution to that of the PEEM-2 microscope, much higher flux and flux

density, a wide spectral range and full capabilities for control of the photon polarization. Figure 1c shows the macro-domain structure of a polystyrene - polymethylmethacrylate (PS/PMMA) (30/70) blend sample, recorded using a photon energy of 285.15 eV, the C 1s → π* peak of PS. The bright continuous signal is PS while the dark discrete domains are PMMA. Due to the high molecular weight (1 MD for PS, 300 kD for PMMA) there is incomplete phase separation, such that the discrete PMMA domains incorporate microdomains of PS with sizes in the 10-200 nm range. Figure 1d is a magnification of a single PMMA domain while Figure 1e is a line profile across one of the smallest PS microdomains in this image, demonstrating a spatial resolution better than 40 nm. This is typical of the spatial resolution capabilities of X-PEEM instruments which do not employ an energy filter or aberration compensation. X-PEEMs with energy filters provide somewhat better energy resolution (*21*). Recently aberration compensation optics that reduce spherical aberrations have been developed for X-PEEM (*20*, *22*). These promise to further improve spatial resolution while also improving the efficiency of the electron optics. The latter is critical for studies of soft matter samples like biomaterials and proteins which are highly sensitive to radiation damage.

Figure 2 presents an experimental measurement of the sampling depth and outlines the analysis of a typical X-PEEM data set from a study of protein (human serum albumin, HSA) adsorbed to a phase segregated polymer (PS/PMMA). We have measured the sampling depth for X-PEEM as applied to proteins on a polymer surface to be 4±1 nm for the 1/e fall-off of the signal based on analysis of the C 1s spectra of uniform PS thin films on a Si wafer (Figure 2a) (*23*) which means the total sampling depth is 10 nm. While the sampling depth does vary with material, due to changes in work function and electron transport in the near surface region, the electronic character of organic polymers and bio-polymers are rather similar and thus both the transport and the work function are likely to be similar in the materials we are studying. The X-PEEM sampling depth of 10 nm can be up to ~ 5 times larger than that of XPS. This is very advantageous for studies of protein-polymer interactions since, at sub-monolayer coverages that are the focus of this work, the protein or peptide adsorbate layer is sufficiently thin (0.5-5 nm) that the underlying polymer biomaterial also contributes significantly to the detected signal. Thus, X-PEEM is an ideal tool for studies of the interface between proteins and solid surfaces since it can simultaneously detect, quantify and map both adsorbate and substrate.

Figures 2b-2g document a typical X-PEEM study, in this case of a PS/PMMA blend exposed for 20 minutes to an aqueous solution of human serum albumin (HSA) at a very low concentration (0.005 mg/mL) (*24*). The PS/PMMA blend was prepared by dissolving PS and PMMA in dichloromethane in a 30:70 weight ratio at a 1 wt% level, then spin casting (4000 rpm, 40 s) onto clean 0.8 cm x 0.8 cm native oxide silicon wafers. The substrates were placed in 50 mL beakers and covered with 5 mL of protein solution. After 20 min, the solutions were diluted with at least 50 mL of distilled, deionized water (DDI), vigorously rinsed and the overlayer water replaced 3 times, while continuously keeping the Si chip covered with water. This avoids passing the substrate through the air-water interface of the original protein solution, which is important since protein typically locates

preferentially at the air-water interface. After rinsing, the remaining water was removed by touching the edge of the Si wafer with lens paper. Since the samples are introduced into the ultrahigh vacuum (UHV) of the X-PEEM via a turbo-pumped load lock, all of the water is ultimately removed and the samples are examined in a dry state.

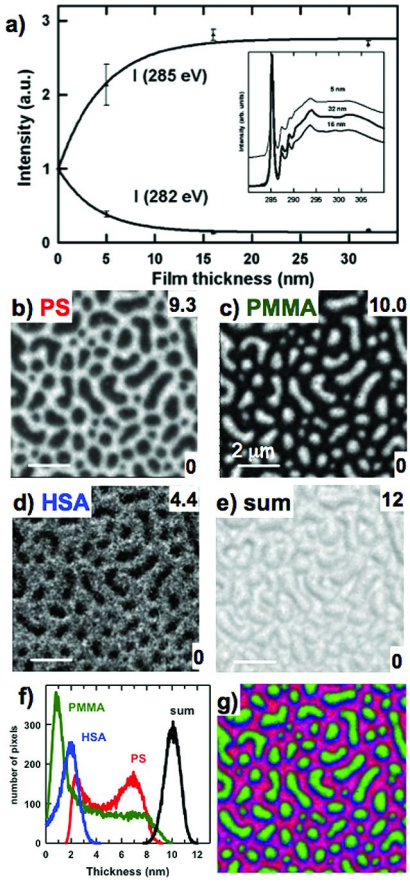

Figure 2. a) Plot of intensity at 282 eV (pre-C 1s, sensitive to the Si substrate) and 285 eV (PS peak) as a function of the thickness of spun-coat films of PS (23).The film thicknesses were measured by atomic force microscopy (AFM) from the profile across a scratch. (b-d) Components maps of a fit of the spectra of PS, PMMA and human serum albumin (HSA) to a C 1s image sequence of a PS/PMMA blend exposed for 20 minutes to a 0.005 mg/ml aqueous solution of HSA. The number at the top right of each map is the maximum of the gray scale for each component map (in each case the minimum is 0). e) Sum of the component maps. The quantitative thickness scales were established by setting the mean of the sum signal to 10 nm. f) histograms of the individual and sum of component maps. g) Rescaled, color coded composite of the PS (red), PMMA (green) and HSA (blue) maps. (see color insert)

In Proteins at Interfaces III State of the Art; Horbett, T., et al.;
ACS Symposium Series; American Chemical Society: Washington, DC, 2012.

This X-PEEM measurement consisted of a sequence of 43 images, each recorded with a 2 sec exposure, with photon energies between 281 and 297 eV. The X-ray beam was shuttered in the 2-3 second interval between each image acquisition in order to reduce radiation damage. After energy calibration (by assigning the C 1s → $\pi^*_{C=C}$ transition of PS to 285.15 eV), the image sequence was normalized to the incident photon flux spectrum which was recorded from a clean Si wafer, with correction for the Si X-ray adsorption and a bolometric term relating to the photon energy dependence of the detector. Reference spectra of PS, PMMA and HSA (*25*) were obtained in separate measurements of the pure materials and placed on absolute intensity scales, as outlined elsewhere (*10*, *12*, *13*). The C 1s image sequence was fit to these quantitative C 1s reference spectra, which results in maps of the spatial distribution of the 3 components (Figures 2b, 2c, 2d). The grayscale range of each component map (indicated by the number at the lower and upper left of each map) indicates the thickness in nm, determined by setting the mean of the sum of all component maps (Figure 2e) to the total sampling depth (10 nm). Figure 2f displays histograms of the quantitative component maps and the sum. The map of the sum has much lower contrast variation than the individual component maps, and the histogram of the sum is relatively narrow, consistent with our assumption that the electron yield and sampling depth are independent of the exact surface composition. Figure 2g is a color coded composite of the 3 component maps with the intensity of each color set to span the full range of each component map. This display clearly shows that the preferred adsorption sites of the HSA protein are the interphase region (the ~100-300 nm band between the PS and PMMA domains), followed by PS, with relatively little protein adsorbed on the PMMA domains, as visualized by a relatively pure green color in those areas. While this example is presented mainly to illustrate the X-PEEM method, data analysis and presentation, the results are very typical of the many protein – polymer blend surfaces we have examined. Except in cases where interactions with a specific domain type are favored by engineered electrostatic interactions (cf the pH dependent results for HSA and sub-6 adsorption to PS/PMMA-PAA (*14*), where the positively charged sub-6 peptide is electrostatically attracted to the negatively charged PAA polymer), we have found that proteins and peptides preferentially adsorb to the interphase (region where domains of different character meet) – polar/non-polar or more/less hydrophobic. We interpret this in terms of more favorable interactions with the more complex environment of the interphase, which allows a wider range of interactions with the multi-functional nature of proteins. Since the adsorption regime (concentrations, time of interactions) is one where the adsorption is partially reversible, the actual surface distributions depend on the length of time of interaction (*24*) and thus both kinetic and thermodynamic factors play a role.

Radiation damage is a severe challenge when applying X-PEEM to protein-polymer interactions. Despite being a full field technique, we estimate the rate of damage relative to signal generation is about 1 order of magnitude higher in X-PEEM than in STXM (*23*). To reduce radiation damage, a shutter with a 0.1 second response time is used to block the X-ray beam during each photon energy step as well as the period of transfer of images from the CCD camera to the acquisition computer. The photon beam is masked upstream of the monochromator to reduce

the incident flux to less than 10% of the maximum. A variable point spacing is used and the number of photon energies is restricted to that which will capture the spectral aspects that differentiate the components of the system studied. Very short exposure times (1 – 2 s) are used to further minimize radiation damage. The relatively rapid radiation damage, combined with the very weak signal from ultra-thin systems such as self-assembled monolayers (SAM) makes such systems very challenging to study – however results have been obtained as indicated below.

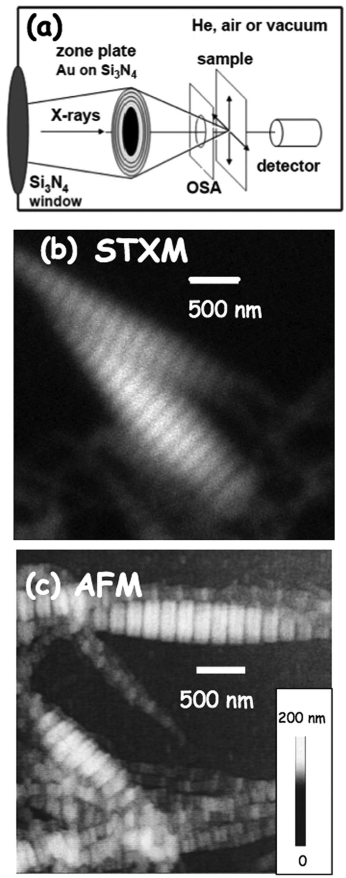

Figure 3. a) schematic of a scanning transmission X-ray microscope (STXM). b) STXM image (OD representation) of a collagen fibril recorded at 288.2 eV, peak of the C 1s → π^*_{amide} transition of collagen. The spatial resolution, as judged by the sharpness of the structure and a Fourier spatial frequency analysis, is 35 nm. c) AFM height image of collagen fibrils in another area on the same sample examined by STXM. (collagen sample and AFM image courtesy of J. Goh)

STXM Applied to Protein–Polymer Interactions

Scanning Transmission X-ray Microscopy (STXM) is a point probe method in which images are obtained serially by mechanically raster scanning the sample though the focal point of a zone plate X-ray lens or (in a few cases) by scanning the zone plate (ZP) and order sorting aperture (OSA) synchronously while the sample is stationary. Figure 3a is a schematic of the functional components of a STXM. The X-ray beam is focused using a Fresnel zone plate (ZP) which is a circular diffraction grating. ZPs have a focal length (f) given by $f = D\delta r/\lambda$ where D is the diameter of the ZP, δr is the width of the outermost zone, and λ is the X-ray wavelength (*11*). The ZPs used in the work reported here had D=240 μm, δr = 25 nm, which gives focal lengths from 1 – 4 mm between 250 and 1000 eV. The focused spot contains only 5-15 % of the X-rays incident on the ZP and thus a scheme to block the un-diffracted (and higher order diffracted) X-rays is needed. This is provided by the combination of a central stop (95 μm diameter, 2 μm thick Au circle at the centre of the ZP), and an order sorting aperture (40-70 μm), which, when properly aligned, blocks all but the first order light. The properties and quality of the zone plate determine the spatial resolution and efficiency of STXM. Over the past 20 years there have been major advances in the fabrication technology such that the present state-of-the-art systems can provide 10 nm spatial resolution with a high contrast test structure (*26*). Figure 3b presents a STXM image of a bundle of collagen. The transverse banding is a well known superstructure in collage (*27*, *28*). Analysis of the Fourier spatial frequencies of this image indicates a spatial resolution of 35 nm. For comparison, Figure 3c presents an atomic force microscopy (AFM) image from elsewhere on the same sample (presented on the same spatial scale).

Comparison of X-PEEM and STXM for Studies of Protein–Polymer Interactions

Although techniques such as atomic force microscopy (AFM) (*29*, *30*) and transmission electron microscopy (TEM) (*31*) have better spatial resolution, X-PEEM and STXM provide much more detailed chemical information through spatially resolved near-edge X-ray absorption fine structure (NEXAFS) spectroscopy (*32*). X-PEEM is an ideal tool to map the distribution of protein on polymeric surfaces since this technique has an optimal near surface sensitivity with a spatial resolution better than 50 nm. Scanning Transmission X-ray Microscopy (STXM) has comparable or perhaps slightly better spatial resolution, and excellent quantitative speciation capabilities, with fewer limitations in terms of this application. A major advantage of STXM over X-PEEM is the ability to examine protein adsorption in the presence of a thin aqueous over layer, thus under conditions much closer to real-world situations than is the case for the UHV, high applied electric field environment of the X-PEEM. However, STXM operates in transmission mode, which integrates the signal through the entire thickness of the sample, and thus it is much less surface sensitive.

For quantitative analyses of surface-adsorbed molecules where the underlying substrate can be mapped simultaneously, X-PEEM is the premier technique. It probes the top 10 nm of the sample, with a sensitivity to adsorbates in the range of 0.1 monolayer or less. Of course there are limitations to X-PEEM as applied to studies of protein interfaces. *In situ* biological experiments using X-PEEM are not possible since relevant biological interactions must be established in an aqueous environment, which is incompatible with the ultra-high vacuum requirement of X-PEEM. To avoid charging artifacts, X-PEEM requires ultra-thin samples of the biomaterial, which can be difficult to prepare. For example polyurethanes are a common medical biomaterial (*33*) but they, along with other cross-linked polymers, are very difficult to spin coat, which is the preferred technique to prepare polymer films sufficiently flat (to avoid topography artifacts) and sufficiently thin (<50 nm) to avoid charging in X-PEEM. In principle it may be possible to use ultramicrotomy to solve this problem, although X-PEEM does require very flat surfaces for optimal imaging. An alternative approach would be to prepare a relevant protein exposed biomaterial on a thick substrate, and then sputter-coat that surface with a layer of metal (Pd, or Pt) that is sufficiently thin to allow the photoelectrons to escape the surface but which is also thick enough to be nearly continuous and sufficiently conducting so as to avoid charging. Gilbert et al. (*34*, *35*) have perfected this approach and applied it to many insulating materials, so as to allow studies of thick sections or bulk samples, including many studies of $CaCO_3$ based biominerals. However it is not clear how well adsorbed proteins and delicate organic substrates would survive the energetic sputter coating process. Further, it would not be possible to study the same substrate before and after protein adsorption.

It is difficult to use NEXAFS spectroscopy to identify different types of proteins in a mixture. One might expect this to be feasible since each amino acid has a unique NEXAFS spectrum (*36*). However, the NEXAFS spectra of all proteins and most peptides tend to be very similar, since they are the average over relatively similar distributions of amino acid residues (*37*). Even so, we have successfully studied competitive protein-peptide adsorption in cases where the peptide contains a special spectral signature arising from an abundance of a specific amino acid, in this case, arginine (*25*). It may be possible to use metal- or quantum-dot-labeled proteins to achieve differentiation of specific components in a mixture of biological adsorbates, although one is always concerned that the label may alter adsorption behavior, and there are sensitivity limitations to soft X-ray microscopy techniques.

Radiation damage is of considerable concern in these experiments due to the high flux of X-rays. Direct comparison of doses in X-PEEM and STXM (*23*) have shown that the dose per spectrum is much larger in X-PEEM than in STXM despite the much more concentrated beam in a STXM (typically a spot size of 30 nm diameter with ~10^7 X-ray/s) than in X-PEEM (typically a spot size of 30 μm diameter with ~10^9 X-ray/s) because the exposure times in STXM (50-100 ms total per spectrum) are much shorter than in X-PEEM (50-500 s per spectrum). In both types of X-ray microscopes it is now routine to shutter the photon beam except during the actual acquisition step. For X-PEEM the shutter is closed between successive images, a period of a few seconds in which the

image is transferred from the camera to the acquisition computer and the photon energy is changed to the next value. There are clearly improvements that can be made, such as more sensitive cameras, faster data transfer, and more rapid photon shutters. In our measurement protocol on PEEM-2 at the ALS we minimize the exposure by preferentially using the 2-bunch mode which has 1/15th the flux of the normal multi-bunch mode operation. We also mask the incident beam to reduce the flux, and keep the dwell times and number of images measured as low as possible, consistent with spectroscopic differentiation. With the undulator based PEEM3 at the ALS we must extensively detune the EPU to keep the incident flux within the levels that the sensitive PMMA and protein materials can tolerate. Sample preparation must also be performed carefully to avoid sharp particulates such as silicon dust from cutting the Si substrate, since particles can cause charging and field emission. Finally, despite the zero cost for peer-reviewed access, synchrotron-based techniques are not readily available for many academic or industrial laboratories, due to the limited number of synchrotron facilities and X-PEEM beamlines.

Despite the aforementioned challenges, X-PEEM and STXM spectromicroscopy methods are providing useful information in the biomaterials area. New developments such as aberration correction (*38–40*) are expected to improve the spatial resolution to ~10 nm in the near future. With 10 nm spatial resolution, imaging individual proteins will become possible. Perhaps more beneficial for this research area, correction of spherical aberration is predicted to increase the transmission of the electron imaging column up to 100-fold which would allow use of smaller apertures in the PEEM column to improve spatial resolution, or enable lower incident fluxes to be used for the same spatial resolution.

For experimental details of materials, sample preparation, data analysis etc, the reader is referred to the original literature cited for each example. All data processing was performed using aXis2000 (*41*).

Examples of Soft X-ray Spectromicroscopy Studies of Protein–Polymer Interfaces

pH-Dependent Protein and Peptide Adsorption to PS-PMMA/PAA

Our studies of albumin, fibrinogen and peptide adsorption to polystyrene-poly(methyl methacrylate) (PS-PMMA) (*24*, *42*, *43*) or PS-polylactide (PLA) films (*15*, *25*, *44*) indicate that hydrophobic interactions are the dominant force determining the preferred sites of adsorption. However, most surfaces analyzed to date using our approach have been neutral and hydrophobic. Recently (*14*) we have explored protein and peptide adsorption to a surface prepared by blending PS with a block co-polymer of poly(methyl methacrylate) and polyacrylic acid (PMMA-b-PAA) to form a phase segregated patterned surface that is negatively charged at neutral pH but which can have the surface charge modified by adjusting the pH, thereby probing the effect of electrostatic interactions with a negatively charged protein and a positively charged peptide as a function of pH. Ultimately

our intent is the use the acrylic acid surface groups in order to chemically functionalize the surface in order to tailor its surface adsorption properties for proteins and peptides.

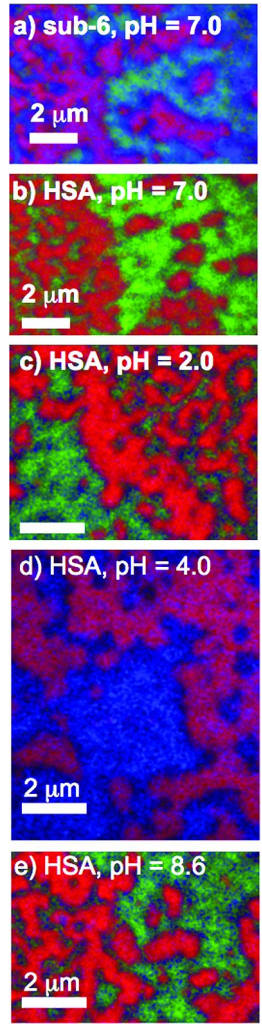

Figure 4. X-PEEM derived color coded composite maps (14) of PS/PMMA-PAA 60:40 exposed to (a) sub-6 protein at pH=7.0; (b-e) 0.05 mg/mL HSA at pH=7.0, 2.0, 4.0 and 8.6. PS is coded red, PMMA-PAA is coded green and HSA or sub-6 is coded blue. In each color coded composite map, the mapping of each color to amount perseveres the overall thickness scale – i.e. the zero of each color scale is set to the minimum over all 3 component maps while the 255 of each color scale is set to the maximum over all 3 component maps (called an 'absolute' presentation). (see color insert)

Figure 4 presents color coded composite images (red = PS, green = PMPA, blue = peptide (Figure 4a) or albumin (Figures 4b-4e)) for surfaces prepared by a 20 minute exposure of a 60:40 (wt %) PS/PMMA-PAA blend to a 0.005 mg/mL aqueous solution of sub-6 peptide and albumin at pH=7.0. Peptide concentrations of 0.005 mg/mL were used for direct comparison to our previous study of SUB-6 adsorption to PS-PMMA (*25*). For each composite map an absolute color coding is used (see caption for details). At neutral pH, SUB-6 is positively charged (+5) while HSA is negatively charged (-15) (*24*). Thus, if electrostatic interactions were a significant factor, one would expect much larger amounts of positively charged peptide to be adsorbed at neutral pH than negatively charged albumin. This is indeed what is found, as seen by comparing Figures 4a and 4b. HSA adsorption is the strongest on the interdomainal interphase between PS and PMMA-PAA, while the central parts of both the PS and PMMA-PAA domains are relatively pure red and green respectively, indicating very little HSA adsorption. The interdomainal interphase is expected to be region with the highest binding capability due to an amphiphillic character and this would explain these observations if thermodynamics controls the interactions. Alternatively it may be that the interphase is the most "kinetically accessible" at short exposure times, where kinetic factors such as the rates of transformation of proteins from less favorable to more favorable conformations/ orientations for bonding may play a role (*24*, *43*).

The much stronger blue color in the composite for SUB-6 adsorption to the PS/PMMA-PAA surface (Figure 4a) indicates the amount of peptide adsorbed is much larger than the amount of protein adsorbed (Figure 4b). The highest intensity is at the interphase between PS and PMMA-PAA. Both the PS and PMMA-PAA domains show peptide adsorption (pink and teal colors) indicating there is significant adsorption of peptide on these regions. The quantitative analysis of these results is presented elsewhere (*14*). Since both HSA and the surface are net negatively charged, repulsive interactions are expected. In fact, adsorption of HSA to the negatively charged PS/PMMA-PAA surface was more than 50% less than to an uncharged PS-PMMA surface at the same concentration (*24*). The positively charged SUB-6 peptide shows the opposite adsorption behavior to HSA with a large peptide thickness at the interphase and negatively charged PMMA-PAA domains. Peptide adsorption to the PS/PMMA-PAA surface was much higher than to an uncharged PS-PMMA surface (*43*). The increased adsorption of SUB-6 on the PS domains of the charged surface compared to neutral surface is most likely due to adsorption to microdomains of PMMA-PAA embedded within the PS domains.

Figure 4c – 4e are color coded composites for 20 minute exposure of a 60:40 (wt %) PS/PMMA-PAA blend surface to a 0.005 mg/mL albumin solution at pH values of 2.0 (c), 4.0 (d) and 8.6 (e). By changing the pH to acid conditions the surface charge is reduced by protonating the carboxylate sites on the PAA domains. At pH 2, HSA is positively charged while the surface is close to neutral. This modified the adsorption of both the protein and the peptide. At the same time as changing the charge at the surface, pH changes the charge and conformation of the albumin in solution. The quantitative chemical maps of the albumin distribution on the pH-modified PS/PMMA-PAA surfaces (Figure 4b-e) reflect

both effects. At pH 4.0, close to the isoelectric point (IP = 4.7 – 5.3) (*45*), HSA is slightly positive while the surface is negatively charged. At pH 8.6, both protein and surface are negatively charged. Due to intramolecular charge interactions HSA exists in five different conformations depending on the pH. These are designated E, F, N, B, and A (*45*). At lower pH, HSA exists in an unfolded and expanded conformation, while at higher pH it is more compact. The maps at pH 2.0 (Figure 4c) and 8.6 (Figure 4e) show a strongly blue interphase region, indicating the highest protein adsorption. Similar amounts were adsorbed at pH 2.0 and 8.6 as shown by similar shades of pink PS and teal PMMA-PAA in both maps. Close to the isoelectric point, at pH 4.0, adsorption to the PMMA-PAA region was so high that almost no green PMMA-PAA color was visible (Figure 4d). The PS region was also strongly pink showing that adsorption was at a maximum at pH 4.0. Previous studies have shown that maximum levels of protein adsorption tend to occur at the isoelectric point where the protein carries no charge and thus exhibits least electrostatic repulsion. HSA adsorption at pH 2.0 and 8.6 was significantly less than at pH 4.0. At pH 4.0, adsorption on PS/PMMA-PAA was significantly higher presumably due to attractive electrostatic interactions. Compared to the (uncharged) PS/PMMA surface (*24*), adsorption on PS/PMMA-PAA was two- to three-fold greater (*14*). At pH 8.6, where HSA is negative, adsorption to the negative PS/PMMA-PAA surface was much greater than to the uncharged PS/PMMA surface. The X-PEEM results for HSA and SUB-6 adsorption on PS/PMMA-PAA spun cast thin films indicate that the adsorption propensity is determined, at least in part, by electrostatic interactions as indicated by the results of adsorption at varying pH.

Effect of Ionic Strength on Adsorption of Albumin to a Polystyrene-Polylactide Blend

Polylactide (PLA), synthesized by ring-opening polymerization of lactide, is a biocompatible and biodegradable synthetic polyester commonly used in tissue engineering and for drug delivery. For scaffold engineering and drug microcapsules, the rate of degradation and controlled release, respectively, can be greatly impacted by combining a non-biodegradable polymer such as polystyrene (PS) (*46*) or polyethylene glycol (PEG) (*47*) with a biodegradable material. Such combinations of biodegradable and nonbiodegradable polymers, known as bioblends, can be a simple, cost-effective means of obtaining a composite with tunable physical or chemical properties (*48*).

Recently we have investigated the adsorption of HSA to the PS/PLA bioblend platform (*15*). That study showed that phase inversion induced by changing the composition of the PS/PLA substrate, did not affected protein adsorption properties. It also showed that surface topography was not a major factor in controlling adsorption, over a range of 35 to 90 nm rms rugosity. Here we summarize the results from that study on the effect of ionic strength on HSA adsorption to PS/PLA, which was investigated by comparing the adsorption of HSA from distilled deionized (DDI) water and phosphate-buffered saline (PBS) solutions.

HSA at concentrations of 0.005, 0.01 and 0.05 mg/mL was adsorbed from DDI water and PBS buffer solutions onto a polystyrene (PS) – polylactide (PLA) 40:60 film that was annealed for 1h at 70 °C. Figure 5 a-f presents the absolute color coded maps for the six films. For the films exposed to HSA in DDI water, the color coded composite maps show that at the highest concentration (Figure 5a), the amount of protein adsorbed is greatest at the interface between the PS and PLA domains. Furthermore, at higher concentrations the maps exhibit more turquoise and pink colors, suggesting slightly higher protein adsorption, while at the lowest concentration (Figure 5c, 5f), there are more green pixels which suggest a more uneven adsorption. For the PBS buffer system (Figure 5 d-f), the composite images show a strong blue color for the 0.05 mg/mL surface. This indicates a high amount of adsorbed protein. The blue color is not as strong for the other images, showing that less HSA adsorbs to the surface as the HSA concentration decreases, or when the adsorption takes place from DDI water.

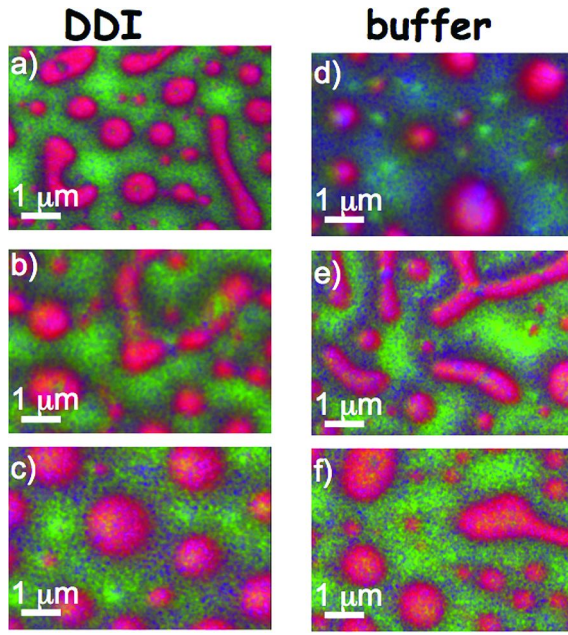

Figure 5. X-PEEM color coded composite maps of 40:60 PS/PLA films (0.7 wt % loading), annealed 1 h at 70 °C exposed to HSA solutions of varying concentrations and from distilled deionized water (DDI) or phosphate saline buffer (PBS) solutions (15): (a, d) 0.05 mg/mL HSA , (b,e) 0.01 mg/mL HSA (rescaled), (c,f) 0.005 mg/mL. The maps on the left (a, b, c) correspond to samples where the solvent was distilled water; the maps on the right (d, e, f) are for samples where the solvent was phosphate buffered saline. PS is coded red, PLA is coded green, and HSA is coded, and the signal from each component is presented on an overall absolute intensity. (see color insert)

Table 1. Thickness (nm) of PS, PLA, and HSA in the PS, PLA and interface regions from PS:PLA 40:60 (0.7 wt%) films annealed 1h at 70 °C exposed to 0.05, 0.01, and 0.005 mg/mL HSA from either DDI water of PBS buffer. Uncertainty ±0.5 nm (*25*)

Region	*Composite*	*HSA adsorbed from DDI*			*HSA adsorbed from PBS*		
	Thickness (nm)	*0.05 mg/mL*	*0.01 mg/mL*	*0.005 mg/mL*	*0.05 mg/mL*	*0.01 mg/mL*	*0.005 mg/mL*
PS	PS	8.1	8.0	9.0	7.8	8.3	9.2
	PLA	0.0	0.9	0.2	0.2	0.3	0.2
	HSA	1.9	1.1	0.8	2.0	1.4	0.7
PLA	PS	2.5	3.0	3.0	2.6	2.5	2.7
	PLA	5.1	6.1	6.7	4.7	6.0	6.5
	HSA	2.4	0.9	0.3	2.8	1.5	0.8
Inter-face	PS	6.5	5.1	3.8	3.9	4.6	4.6
	PLA	0.7	3.1	4.5	2.0	2.5	2.7
	HSA	2.7	1.8	1.7	4.1	3.5	2.8

The quantitative results from the curve fitting of the C 1s spectra extracted from the PS, PLA and interphase domains are summarized in table 1. This analysis show that at all concentrations examined, HSA adsorption occurs most strongly at the interface between PS and PLA. As the protein concentration decreases the average thickness of HSA on the surface also decreases. The quantitative results for the PBS buffer system also show preferential HSA adsorption to the interface between PS and PLA domains. However, the extracted average thickness values of the adsorbed HSA in the interfacial region are almost twice as large compared to adsorption from DDI water for all three concentrations. The X-PEEM results show a correlation between the thickness of the adsorbed protein layer and the ionic strength. This seemingly conflicts with literature reports which show the amount of adsorbed protein decreases with increasing salt concentration on silica, pegylated Nb_2O_5 and $Si(Ti)O_2$ surfaces, as examined with neutron reflectivity (*49*), optical waveguide light mode spectroscopy (*50*) and integrated optical methods (*51*), respectively. Importantly, according to the integrated optical methods, although the number of adsorbed protein molecules decreased with increasing ionic strength, the area occupied by the adsorbed molecules increased with increasing salt concentration. Thus, the increased HSA thickness detected by X-PEEM for PBS buffer system may reflect a conformational change resulting in an increase in the adsorbed protein size without changing the number of adsorbed HSA molecules.

To further investigate this system and to verify if a conformational change was present, the same systems were investigated with ^{125}I radiolabeled HSA which provides a means of measuring the number of adsorbed molecules on the polymer surface. Figure 6 presents a comparison of the X-PEEM and ^{125}I radiolabeling

results, while the data from the radiolabeling experiments are presented in table 2. We used the values for the X-PEEM interfacial region to clearly highlight that there is a difference between adsorption from DDI and PBS using both methods. This comparison shows that at the two higher HSA concentrations (0.05 and 0.01 mg/mL) the number of protein molecules adsorbed from DDI water was almost double that from buffer, while at lower HSA concentration (0.005 mg/mL) the numbers of adsorbed HSA were similar. These results contrast strikingly with the X-PEEM data which showed increasing thickness with increasing ionic strength. Thus, using a combination of X-PEEM and radiolabeling experiments, we concluded that the conformation of HSA adsorbed from buffer is extended relative to that adsorbed from DDI water.

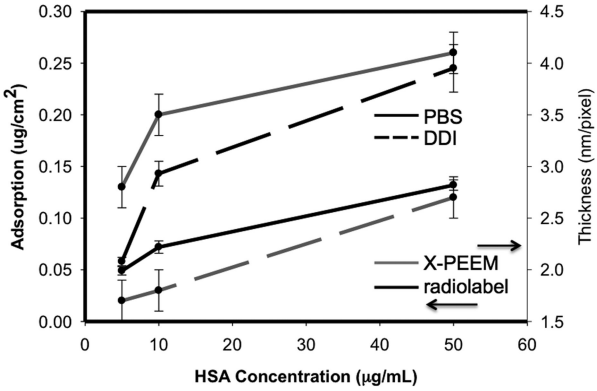

Figure 6. Adsorption isotherms for albumin adsorption from DDI and buffer on 40:60 PS/PLA films (0.7 wt % loading), measured by X-PEEM and ^{125}I radiolabelling (15). PBS is solid and DDI is dashed. X-PEEM detected thickness (right y-axis) is plotted in gray, radiolabeling (left y-axis) in black.

Effect of Hydration on Adsorption of HSA to PS/PMMA

There are concerns that the lateral spatial distributions measured in the dry, UHV conditions in X-PEEM could be different from those which may exist at the fully hydrated polymer surface. This could be a result of modifications of surface distributions in the last stages of drying for example. Although it has lower surface sensitivity than X-PEEM it is possible to measure proteins at polymer surfaces in STXM, since the polymer films have to be quite thin (<100 nm) to allow for partial penetration of the soft X-rays. In order to investigate the effect of surface hydration, we used STXM to image a HSA hydrated sample formed by sandwiching a thin film of PS-PMMA between two X-ray transparent silicon nitride windows (*16*). This system was examined under completely hydrated, washed and hydrated, and completely dried conditions. Figure 7a-c shows the component maps of PS, PMMA and HSA in the fully hydrated sample, while Figure 7d presents a color coded composite of these component maps (PS, PMMA and HSA are color coded in red, green and blue, respectively;). The lighter pixels

in Figure 7c reveals the areas that correspond to high adsorption of HSA. There is a strong correlation between the areas of high protein and the PMMA domains. Also, the color coded composite shows there is a high density of adsorbed HSA is seen at the interphase between PS and PMMA domains. Figures 7e-h present the corresponding results for the washed, dried and rehydrated system. The results are rather similar to those for the fully hydrated sample.

Table 2. Adsorption of albumin from ^{125}I radiolabelling measurements on PS-PLA (μg/cm²) from distilled water (DDI) versus phosphate buffered saline (PBS). Data shown are the mean of 4 replicates with standard deviation in parentheses (sd, n = 4) (*25*)

	Surface density *(μg/cm²) (sd)*	
Solution concentration (mg/mL)	*DDI*	*PBS*
0.005	0.058 (0.004)	0.049 (0.004)
0.01	0.143 (0.012)	0.072 (0.006)
0.05	0.245 (0.023)	0.132 (0.005)

Figure 7i-k displays the images for the dry system. Compared to the completely wet system, the color coded composite map of the dry surface (Figure 7k) shows a much pinker map, indicating there is more protein on the PS region. The quantitative results show that for the dehydrated system, the spatial distribution of the adsorbed protein is: interdomainal > PS > PMMA. This trend is similar to that observed for HSA adsorption on PS-PMMA as imaged with X-PEEM (*42*). Since X-PEEM probes only the top 10 nm of the surface while STXM samples through the entire film the percentages of adsorbed HSA are higher in the X-PEEM data. The data between STXM and X-PEEM cannot be directly compared, however the relative ratios of the amount of HSA adsorbed to the PS region, PMMA region and interface can be compared. Similar ratios are seen for STXM and X-PEEM dry samples, but the distributions on the washed and fully hydrated samples are different, with a greater amount of HSA adsorbed to the PMMA domains.

The quantitative results for the hydrated system (see table 3) show adsorbed protein thicknesses in excess of 10 nm on the PMMA domains which suggest that there may possibly be bilayer adsorption since the crystallographic dimensions of HSA are 8x8x3 nm. Nonetheless, this adsorbed HSA is only loosely bound to the PMMA domains since a large percentage of the protein was removed upon washing. Washing with 30 uL of DDI water reduced the thickness of HSA adsorbed on the PMMA domains by 50%. By using X-ray spectromicroscopy to examine HSA adsorption under wet and dry conditions, qualitative insight was gained into the adsorption behavior of HSA on chemically heterogeneous surfaces. Moreover, by washing the HSA system, further information on the strength of HSA adsorption was also elucidated.

Table 3. Average thickness (nm) of HSA on PS, PMMA and PS/PMMA interdomainal regions (*16*)

Region	*Component*	*Hydrated (STXM)* (nm/pixel)	(%)	*Washed (STXM)* (nm/pixel)	(%)	*Dry (STXM)* (nm/pixel)	(%)	*Dry (X-PEEM)* (%)
PS	PS	19.5	50	16.7	51	13.9	60	65
	PMMA	14.5	37	11.5	35	6.6	28	14
	HSA	4.7	12	4.6	14	2.7	12	21
PMMA	PS	7.5	15	7.1	18	1.9	8	23
	PMMA	31.9	64	27.4	69	19.4	82	64
	HSA	10.6	21	5.4	14	2.3	10	13
Interdomainal region	PS	4.3	10	9.2	26	4.6	18	38
	PMMA	27.6	66	19.5	55	16.1	63	37
	HSA	10.2	24	6.7	19	4.8	19	25
(HSA ratios PS/PMMA/Interphase)		0.4/1.0/1.0		1.1/1.0/1.2		1.2/1.0/1.9		1.6/1.0/1.9

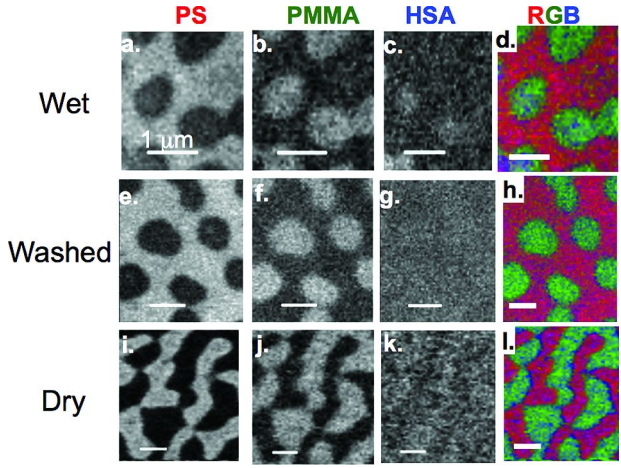

Figure 7. (top) Component maps derived from C 1s STXM image sequences measured from (16): fully hydrated wet cell of HSA adsorbed to a PS-PMMA thin film: (a) PS, (b) PMMA, (c) HSA, and (d) rescaled color composite map. (center) Component maps from a fully hydrated sample, but washed repeatedly with DDI water prior to sealing the wet cell: (e) PS, (f) PMMA, (g) HSA, and (h) rescaled color composite map. (bottom) Component maps from HAS adsorbed to PS-PMMA, washed with DDI water after 20 min exposure and air-dried: (i) PS, (j) PMMA, (k) HSA, and (l) rescaled color composite map. In each case, the color coding for the composite maps is: red, PS; green, PMMA; blue, HSA. HSA = 0.005 mg/mL. (see color insert)

STXM Study of Fibrinogen Adsorption on a Reinforced Polyurethane under Fully Hydrated Conditions

Polyurethanes are commonly used in medical applications due to their favourable mechanical and chemical properties. In a very early exploration of the potential for soft X-ray microscopy to contribute to the field of protein-polymer interface studies (*17*), we investigated the adsorption of fibrinogen to a complex multi-component polyurethane in which the polyether-rich toluene-di-isocyante (TDI) polyurethane matrix was reinforced with two types of more rigid polymer particles, styrene-b-acrylonitrile (SAN) particles and poly-isocyanate poly-addition product (PIPA, a methylene diphenyl diisocyanate

(MDI)-based hard segment-like material) particles. STXM studies of the chemistry and morphology of the polyurethane was reported separately (*52*). In this study the protein distributions determined after the sample was rinsed and dried were compared to those determined with a pure aqueous overlayer (the sample was dried then rehydrated), and with the protein solution as the overlayer (i.e. an '*in situ*' measurement).

Figure 8a displays the color coded composite of component maps derived from a C 1s image sequence of the dry sample. The substrate was a microtomed polyurethane sample embedded with poly(styrene-co-acrylonitrile) (SAN) and poly-isocyanate poly-addition product (PIPA) nanoparticles imaged with STXM. The surface was exposed to 0.1 mg/mL of fibrinogen for 20 min and then rinsed and air dried. SAN, PIPA, Fg and polyurethane are color coded as red, green, blue and black respectively. Figure 8a shows that Fg strongly prefers to adsorb at the interface between SAN and the polyurethane matrix. Figure 8b shows the fit of the C 1s spectrum extracted from those pixels with relatively large Fg content. A distinct shoulder is observed at 288.2 eV, the energy of the dominant C 1s → π^*_{amide} transition of the protein. Also, the quality of the fit without including the Fg reference spectrum is significantly worse.

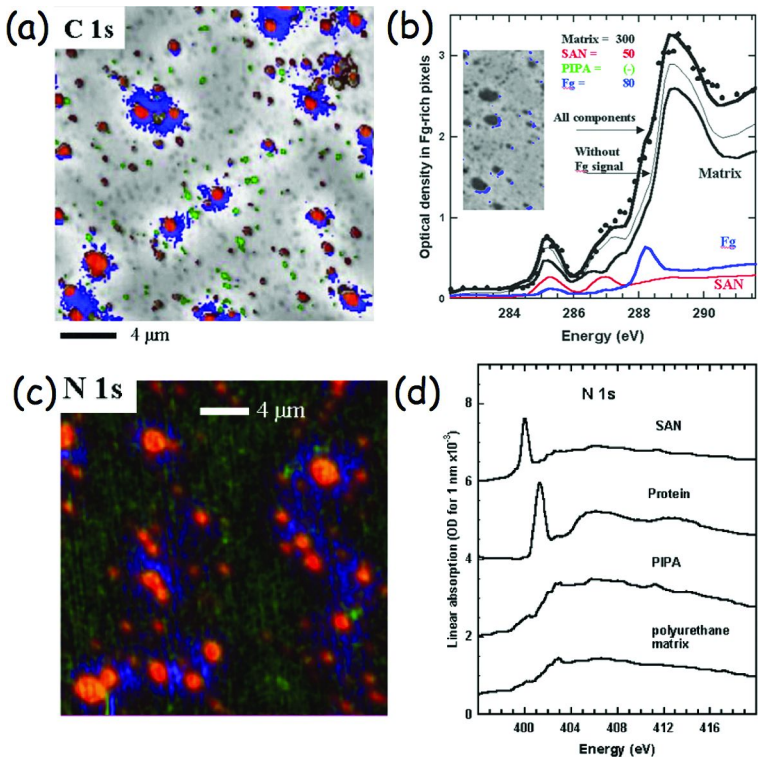

Figure 8. (a) color coded composite of the component maps of the matrix and reinforcing particles in a polyurethane (red = SAN , green = PIPA; grey-scale = matrix) and the adsorbed fibrinogen (Fg, blue), derived from fits to a C 1s image sequence recorded with STXM from a 0.1 mg/mL solution of Fg in phosphate buffer (17). The measurements were performed with the sample in a wet state covered in the buffer solution of the protein. (b) Fit of the C 1s spectrum of the blue pixels. (c) color composite of maps of SAN, PIPA and Fg derived from fits to a C 1s image sequence. (d) Fit of the N 1s spectrum of the blue pixels. (see color insert)

A second sample with the dried Fg rehydrated with water and imaged under fully hydrated conditions showed that Fg preferred to adsorb to the matrix over the SAN. Figure 8c shows the color coded composite derived from a N 1s image sequence. The N 1s edge is particularly sensitive to protein since only the SAN particles have significant amount of nitrogen. The N 1s spectrum of the nitrile component is very different from that of the protein (Figure 8d) and thus the protein is clearly differentiated. As found for the dried sample, the fibrinogen has a very strong affinity for the interface between SAN and the polyurethane matrix. Since Fg has dimensions of 45 x 9 x 6 nm, determined by electron microscopy (*53*), the Fg may be adsorbed end-on to the surface rather than side-on. While the mechanism of Fg adsorption to the interface is not clear, the surface topography may be playing a role since the SAN particles protrude up to 50 nm from the surface. Previous studies by Rechendorff et al. (*54*) found a correlation between surface roughness and increased Fg adsorption.

X-PEEM and TOF-SIMS Study of Peptide Adsorption to a SAM Microarray

Castner and co-workers (*55*) are exploring methods to create surface patterned chemistry for micro-array based medical diagnostics (*56*). One approach is to use a focused ion beam (or irradiation through a mask) to remove parts of a uniform self-assembled monolayer (SAM), followed by filling the removed regions with a second type of SAM. Surface and interface sensitive methods are needed to examine the fidelity of these SAM micro-arrays, as well as the specificity of protein or peptide adsorption to them. In collaboration with Castner and Weidner, we have used X-PEEM to examine adsorption of LKα14 (Ac-LKKLLKLLKKLLKL-OH, a model α-helix peptide) on to a patterned micro-array consisting of alternating squares of an alcohol-terminated SAM (1-thiol-undecanol MCU) and a carboxylate terminated SAM (1-thiol-dodecylcarboxylate, MUDA). Similar samples were also examined using TOF-SIMS. Figure 9a shows a TOF-SIMS image based on the $C_3H_5^+$ ion. The brighter areas correspond to alcohol-rich MCU, while the darker areas correspond to the carboxylate-rich MUDA. For most of the pattern the individual squares are 10 μm x 10 μm while the upper left square has a finer scale pattern (1 μm x 1 μm). Figure 9b shows a TOF-SIMS image derived from the $C_5H_{10}N^+$ ion, which can only have originated from the peptide. The reversal of contrast between these two TOF-SIMS images indicates the peptide is predominantly adsorbed to the MUDA domains. Figure 9c is the ratio of X-PEEM images recorded at 400 eV and 280 eV, which samples net carbon. The bright regions in the X-PEEM image are the carbon-rich MCU domains and the image contrast is similar to that in Figure 9a. A C 1s image sequence was recorded from the intersection of four of the large squares. Preliminary X-PEEM results are shown in Figure 9e-h. Fitting to C 1s reference spectra of MCU, MUDA and the LKα14 peptide (Figure 9d, measured from pure thin films using electron yield NEXAFS at NSLS I) gave the component maps shown in Figures 9e-g. Figure 9h is the peptide component map from fitting a N 1s image sequence to the N 1s spectrum of LKα14 and a constant (the constant represents the C 1s signal of the underlying SAM materials, and has a mapsimilar to that of Figure 9e). The X-PEEM results support the conclusion from TOF-SIMS that the peptide

is adsorbed predominantly on the MUDA, carboxylate-terminated domains. However, these early results also suggest that the underlying SAM domains are not pure, but exists as a mixture of both types of SAMs. This suggests that the Bi^+ bombardment used to remove the MCU was only partly successful and / or the MCU SAM molecules can redistribute during the preparation of the MUDA SAM component.

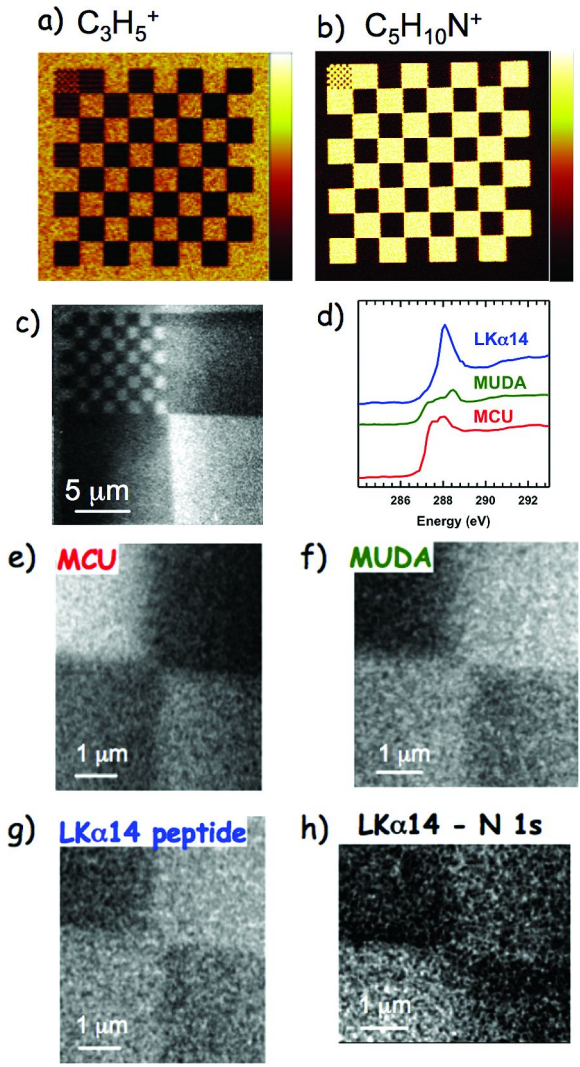

Figure 9. (a) TOF-SIMS image of the surface distribution of $C_3H_5^+$ from a patterned micro-array consisting of alternating squares of an alcohol-terminated SAM (MCU) and a carboxylate terminated SAM (MUDA), exposed to a 0.05 mg/mL solution of LKα14, an alternating leucine (L), lysine (K) peptide, Ac-LKKLLKLLKKLLKL-OH, which is a model α-helix peptide. The brighter pads correspond to the carboxylate terminated MUDA domains while the darker

In Proteins at Interfaces III State of the Art; Horbett, T., et al.;
ACS Symposium Series; American Chemical Society: Washington, DC, 2012.

pads correspond to the alcohol terminated MCU domains. (b) TOF-SIMS image of surface distribution of $C_5H_{10}N^+$ which originates from the peptide. The contrast indicates the peptide is predominantly adsorbed to the MUDA domains. (c) X-PEEM image from the C 1s signal [I(400 eV) – I(280 eV)]. The contrast is the same as that in the TOF-SIMS image of $C_3H_5^+$ indicating it is dominated by substrate signals. (d) C 1s NEXAFS spectra of MCU, MUDA and LKα14 indicting the characteristic features of alcohols, carboxylates and amides in the 287-290 eV region. (e-g) Component maps of MCU, MUDA and LKα14 derived from a fit to a C 1s image sequence (282-293 eV). (h) Map of LKα14 derived from a fit to a N 1s image sequence (396-420 eV). (see color insert)

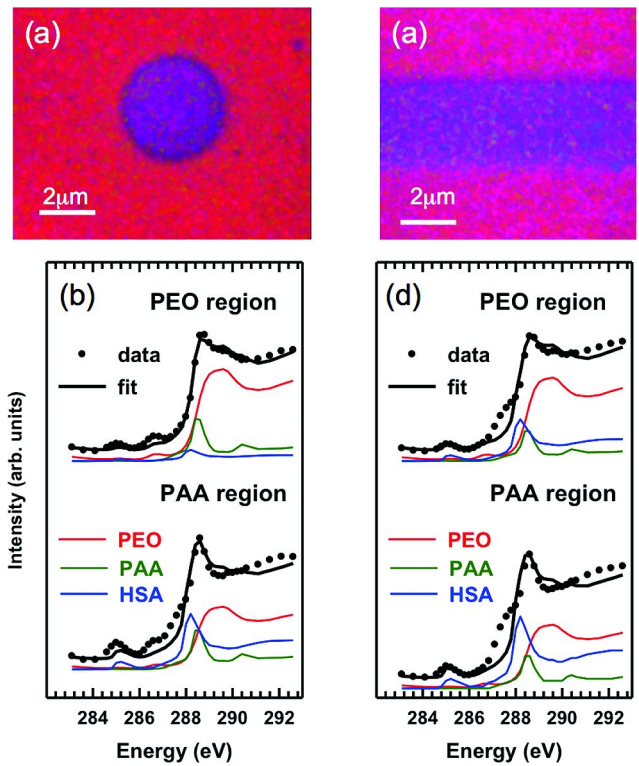

Figure 10. (a) Absolute color component maps for 0.002 mg/ml ubiquitin adsorbed to a PEO-like/ppAA circular microstructure (18). (b) Spectral fitting for the PEO-rich region (top) and ppAA-rich region (bottom). (c) Absolute color component maps for 0.002 mg/ml ubiquitin adsorbed to a PEO/ppAA linear microstructure (18). (d) Spectral fitting for the PEO-rich region (top) and ppAA-rich region (bottom). For all images and spectra, PEO-like is color-coded as red, ppAA is color-coded as green and ubiquitin is color-coded as blue. (see color insert)

X-PEEM Study of Ubiquitin Adsorbed to Microbeam-Patterned Polymeric Surfaces

Materials used for biological applications can be improved through surface modification which can selectively increase or reduce the interaction of the material with biological entities such as proteins, cells, or bacteria (*57–59*). Among the different surface functionalization methods, plasma deposition and plasma grafting techniques have gained considerable popularity for producing surfaces suitable for biomolecule immobilization to elicit specific biological responses (*60*, *61*). For example, surfaces containing COOH and NH_2 functionalities are widely used to bind protein (*62*) and for cell growth assays (*63*). In a recent study, X-PEEM was used to investigate protein adsorption on micro-structured polymers fabricated by e-beam lithography and plasma polymerization (*18*). Ubiquitin was used as model protein because of its relatively simple structure. Ubiquitin, is a highly ubiquitous protein present in all eukaryotes, while it is absent from prokaryotes. Ubiquitin is a 76 amino acid residue protein. It is the most highly conserved protein known thus far. It has a molecular weight of 8.564 kDa and an isoelectric point of 6.79. Ubiquitin labels proteins for proteosomal degradation. Through this means, ubiquitination controls the stability, function, and intracellular localization of a wide variety of proteins (*64*).

Micropatterned structures consisting of plasma polymerized acrylic acid (ppAA) circular domains within a background of a polyethylene oxide (PEO) -like protein resistant material were fabricated by electron beam lithography and plasma polymerization. 0.002 mg/mL ubiquitin was adsorbed to the surface and then imaged with X-PEEM. Figure 10 shows the absolute color coded composites of component maps derived from C 1s X-PEEM image sequences for a circular (Figure 10a) and a linear (Figure 10b) pattern. In these maps, PEO is color coded red, ppAA is color coded green and ubiquitin is color coded blue. The matrix is intensely red, which is indicative of low protein adsorption while the ppAA circular domains are purple, which arises from a roughly equal amount of red PEO and blue protein. These results show that PEO dominates the entire surface. Even under the thin layer of ppAA, a large amount of PEO can be detected. These mapping results were verified by quantitative curve fit analysis of spectra extracted from the two substrate domains (see Table 4). Only a small amount (22-25%) of ppAA was detected by X-PEEM. Nonetheless, even though the ppAA layer is thin, selective adsorption of ubiquitin is seen on the surface. On the protein resistant PEO-like surface, only 6% of protein is present, while on the ppAA-rich area, 32% of protein is found at the center of the circle. The spectral results show a good fit for the PEO-rich areas. However a poor fit is seen for the ppAA-rich region, where there seems to be a missing component below C1s → $\pi^*_{C=O}$ which may be the result of radiation damage or contamination. In the case of the line pattern, the quantitative spectral fitting (Figure 10d) shows poor fits for both the PEO-like and ppAA-rich regions. A missing component is clearly seen at ~287 eV. Based on our knowledge of C 1s NEXAFS spectroscopy, this missing component is indicative of a hydrocarbon (C-H) signal and is assumed arise from some source of contamination which is currently unidentified. This

spectral mismatch may be the reason why ppAA is shown to be only a minor component while XPS results of the same system suggest that the ppAA layer is greater than 10 nm. Further investigations are required to clarify this discrepancy.

Table 4. Percentage of PEO-like, ppAA, and ubiquitin on PEO-like/ppAA microstructures for PEO-rich and PAA-rich areas for films exposed to 0.002 mg/mL ubiquitin. Uncertainty ±5% (*18*)

		Percentage	
Region	*Component*[(a)]	*Circle*	*Line*
PEO-like	PEO	69%	59%
	ppAA	25%	17%
	Ubiquitin	6%	24%
ppAA	PEO	46%	36%
	ppAA	22%	14%
	Ubiquitin	32%	50%

[(a)] reference spectra used to derive these results were: PEO-like, ppAA as ppAA and ubiquitin as albumin.

Summary

Through these examples it is clear that soft X-ray spectromicroscopy is making significant contributions to our understanding of protein and peptide interactions with spontaneously or artificially phase segregated polymer surfaces, of the type frequently encountered in biomaterials used for medical and other applications. While this chapter has focused on recent results from our group, there are others using these techniques. For example, Turgeon and coworkers (*65*, *66*) have applied X-PEEM to investigate the integrity of fluorocarbon coatings on stents, while Kappen et al. (*67*) have used X-PEEM to study copper and polypyrrole micro-patterns deposited on fluorocarbon substrates, in order to elucidate growth mechanisms, elemental distributions, topography, local conductivity and thin film orientation. An up-to-date listing of current and projected soft X-ray microscopes has recently been published (*13*) – there are about 50 such facilities world-wide, all of which are publically accessible, with access determined on a peer-reviewed competitive basis. With ever increasing numbers of 3rd generation synchrotron facilities, almost all of which feature beamlines dedicated to X-PEEM and STXM, the potential for applying soft X-ray microscopy to studies of protein interfaces is enormous.

Acknowledgments

We thank the Hancock Research Group from UBC for providing the SUB-6 peptide. We thank J. Goh for providing the collagen sample and AFM images. We thank D. Castner and T. Weidner for providing the SAM micro-array samples, the C 1s reference spectra and the TOF-SIMS results. This research was supported by the Natural Sciences and Engineering Research Council (NSERC, Canada), AFMNet and the Canada Research Chairs program. X-ray microscopy was carried out using PEEM2, PEEM3 and STXM5322 at the ALS and the CaPeRS PEEM and STXM at the CLS. The ALS is supported by the US Department of Energy under Contract DE-AC03-76SF00098. The CLS is supported by NSERC, CIHR, NRC and the University of Saskatchewan. We thank the staff scientists, David Kilcoyne and Tolek Tyliszczak (ALS) and Jian Wang, Uday Lanke and Chithra Karunakaran (CLS) for their expert support of the beamlines and microscopes.

References

1. Castner, D. G.; Ratner, B. D. *Surf. Sci.* **2002**, *500*, 28–60.
2. Anderson, J. M.; Rodriguez, A. D.; Chang, T. *Semin. Immunol.* **2008**, *20*, 86–100.
3. Frey, B. L.; Jordan, C. E.; Komguth, S.; Com, R. M. *Anal. Chem.* **1995**, *67*, 4452–4457.
4. Veiseh, M.; Zareie, M. H.; Zhang, M. *Langmuir* **2002**, *18*, 6671–6678.
5. Roach, L. S.; Song, H.; Ismagilov, R. F. *Anal. Chem.* **2005**, *77*, 785–796.
6. Wadu-Mesthrige, K.; Xu, S.; Amro, N. A.; Liu, G. Y. *Langmuir* **1999**, *15*, 8580–8583.
7. Rezwan, K.; Meier, L. P.; Gauckler, L. J. *Biomaterials* **2005**, *26*, 4351–4357.
8. Norde, W.; Lyklema, J. *J. Biomater. Sci., Polym. Ed.* **1991**, *2*, 183–202.
9. Haynes, C. A.; Norde, W. *Colloids. Surf., B* **1994**, *2*, 517–566.
10. Leung, B. O.; Brash, J. L.; Hitchcock, A. P. *Materials* **2010**, *3*, 3911–3938.
11. Howells, M.; Jacobsen, C.; Warwick, T. Principles And Applications of Zone Plate X-Ray Microscopes. In *Science of Microscopy*; Hawkes, P. W., Spence, J. C. H., Eds.; Springer, New York, 2007.
12. Ade, H.; Hitchcock, A. P. *Polymer* **2008**, *49*, 643–675.
13. Hitchcock, A. P. Soft X-ray Imaging and Spectromicroscopy. In *Handbook on Nanoscopy*; Van Tendeloo, G., Van Dyck, D., Pennycook, S. J., Eds.: Wiley: New York, 2012; Volume 2, pp 745−791.
14. Leung, B. O.; Hitchcock, A. P.; Cornelius, R. M.; Brash, J. L.; Scholl, A.; Doran, A. *J. Electron Spectrosc. Relat. Phenom.* **2012** DOI: 0.1016/j.elspec.2012.06.004.
15. Leung, B. O.; Hitchcock, A. P.; Brash, J. L.; Scholl, A.; Doran, A. *Biomacromolecules* **2009**, *10*, 1838–1845.
16. Leung, B. O.; Wang, J.; Brash, J. L.; Hitchcock, A. P. *Langmuir* **2009**, *25*, 13332–13335.
17. Hitchcock, A. P.; Morin, C.; Heng, Y. M.; Cornelius, R. M.; Brash, J. L. *J. Biomater. Sci., Polym. Ed.* **2002**, *13*, 919–938.

18. G. Ceccone, G.; Leung, B. O.; Perez-Roldan, M. J.; Valsesia, A.; Colpo, P.; Rossi, F.; Hitchcock, A. P.; Scholl, A. *Surf. Interface Anal.* **2010**, *42*, 830–834.
19. Anders, S.; Padmore, H. A.; Duarte, R. M.; Renner, T.; Stammler, T.; Scholl, A.; Scheinfein, M. R; Stohr, J.; Seve, L.; Sinkovic, B. *Rev. Sci. Instrum.* **1999**, *70*, 3973–3981.
20. Feng, J.; Forest, E.; MacDowell, A. A.; Marcus, M.; Padmore, H.; Raoux, S.; Robin, D.; Scholl, A.; Schlueter, R.; Schmid, P.; Stöhr, J.; Wan, W.; Wei, D. H.; Wu, Y. *J. Phys C: Condens. Matter* **2005**, *17*, S1339–S1350.
21. Christensen, S. L.; Haines, B. M.; Lanke, U. D.; Paige, M. F.; Urquhart, S. G. *IBM J. Res.* **2011**, *55*, 5:1–5:6.
22. Schmidt, Th.; Marchetto, H.; Lévesque, P. L.; Groh, U.; Maier, F.; Preikszas, D.; Hartel, P.; Spehr, R.; Lilienkamp, G.; Engel, W.; Fink, R.; Bauer, E.; Rose, H.; Umbach, E.; Freund, H.-J. *Ultramicroscopy* **2010**, *110*, 1358–1361.
23. Wang, J.; Li, L.; Morin, C.; Hitchcock, A. P.; Doran, A.; Scholl, A *J. Electron Spectrosc.* **2009**, *170*, 25–36.
24. Li, L.; Hitchcock, A. P.; Robar, N.; Cornelius, R.; Brash, J. L.; Scholl, A.; Doran, A. *J. Phys. Chem B* **2006**, *110*, 16763–16773.
25. Leung, B. O.; Hitchcock, A. P.; Brash, J. L.; Scholl, A.; Doran, A.; Henklein, P.; Overhage, J.; Hilpert, K.; Hale, J. D.; Hancock, R. E. W. *Biointerphases* **2008**, *3*, F27–F35.
26. Chao, W.; Fischer, P.; Tyliszczak, T.; Rekawa, S.; Anderson, E.; Naulleau, P. *Opt. Express* **2012**, *20*, 9777–9783.
27. Wen, C. K.; Goh, M. C. *Proteins* **2006**, *64*, 227–233.
28. Shoulders, M. D; Raines, R. T. *Ann. Rev. Biochem.* **2009**, *78*, 929–958.
29. Siedlecki, C. A.; Marchant, R. E. *Biomaterials* **1998**, *19*, 441–454.
30. Ta, T. C.; McDermott, M. T. *Anal. Chem.* **2000**, *72*, 2627–2634.
31. Sousa, A.; Sengonul, M.; Latour, R.; Kohn, J.; Libera, M. *Langmuir* **2006**, *22*, 6286–6292.
32. Stöhr, J. NEXAFS Spectroscopy. In *Springer Tracts in Surface Science*; Springer: Berlin, 1992; Vol. 25.
33. Xu, L.-C.; Runt, J.; Siedlecki, C. A. *Acta Biomater.* **2010**, *6*, 1938–1947.
34. Gilbert, B.; Margaritondo, G.; Douglas, S.; Nealson, K. H.; Edgerton, R. F.; Rempfer, G.; De Stasio, G. *J. Electron.. Spectrosc. Relat. Phenom.* **2001**, *114/116*, 1005–1009.
35. De Stasio, G.; Frazer, B. H.; Gilbert, B.; Richter, K. L.; Valley, J. W. *Ultramicroscopy* **2003**, *98*, 57–62.
36. Zubavichus, Y.; Shaporenko, A.; Grunze, M.; Zharnikov, M. *J. Phys. Chem. Lett.* **2005**, *109*, 6998–7000.
37. Stewart-Ornstein, J.; Hitchcock, A. P.; Hernàndez-Cruz, D.; Henklein, P.; Overhage, J.; Hilpert, K.; Hale, J.; Hancock, R. E. W. *J. Phys. Chem. B* **2007**, *111*, 7691–7699.
38. Wichtendahl, R.; Fink, R.; Kuhlenbeck, H.; Preikszas, D.; Rose, H.; Spehr, R.; Hartel, P.; Engel, W.; Schlögl, R.; Freund, H.-J.; Bradshaw, A. M.; Lilienkamp, G.; Schmidt, Th.; Bauer, E.; Brenner, G.; Umbach, E. *Surf. Rev. Lett.* **1998**, *5*, 1249–1256.

39. Schmid, P.; Feng, J.; Padmore, H. A.; Robin, D.; Rose, H.; Schlueter, R.; Wan, W.; Forest, E.; Wu, Y. *Rev. Sci. Instrum.* **2005**, *76* (1-14), 023302.
40. MacDowell, A. A.; Feng, J.; DeMello, A.; Doran, A.; Duarte, R.; Forest, E.; Kelez, N.; Marcus, M. A.; Miller, T.; Padmore, H. A.; Raoux, S.; Robin, D.; Scholl, A.; Schlueter, R.; Schmid, P.; Stöhr, J.; Wan, W.; Wei, D. H.; Wu, Y. *AIP Conf. Proc.* **2007**, 1341–1344.
41. Hitchcock, A. P. aXis2000 is free for non-commercial use. It is written in Interactive Data Language (IDL) and available from http://unicorn.mcmaster.ca/aXis2000.html, 2012.
42. Morin, C.; Hitchcock, A. P.; Cornelius, R. M.; Brash, J. L.; Scholl, A.; Doran, A. *J. Electron. Spectrosc. Relat. Phenom.* **2004**, *137-140*, 785–794.
43. Li, L.; Hitchcock, A. P.; Cornelius, R.; Brash, J. L.; Scholl, A.; Doran, A. *J. Phys. Chem B* **2008**, *112*, 2150–2158.
44. Leung, B. O.; Hitchcock, A. P.; Brash, J. L.; Scholl, A.; Doran, A. *Macromolecules* **2009**, *42*, 1679–1684.
45. Foster, J. F. In *Albumin Structure, Function and Uses*; Rosenoer, V. M., Oratz, M., Rothschild, M. A., Eds.; Pergamon: Oxford, 1977; pp 53−84.
46. Saravanan, M.; Bhaskar, K.; Srinivasa, R. G.; Dhanaraju, M. D. *J. Microencapsulation* **2003**, *20*, 289–302.
47. Cai, Q.; Bei, J.; Wang, S. *Polym. Adv. Technol.* **2002**, *13*, 534–540.
48. Zhang, G.; Zhang, J.; Wang, S.; Shen, D. *J. Polym. Sci., Part B: Polym. Phys.* **2003**, *41*, 23–30.
49. Su, T. J.; Lu, J. R.; Thomas, R. K.; Cui, Z. F.; Penfold, J. *J. Colloid Interface Sci.* **1998**, *203*, 419–429.
50. Pasche, S.; Voros, J.; Griesser, H. J.; Spencer, N. D.; Textor, M. *J. Phys. Chem. B* **2008**, *109*, 17545–17552.
51. Ramsden, J. J.; Prenosil, J. E. *J. Phys. Chem.* **1994**, *98*, 5376–5381.
52. Rightor, E. G.; Urquhart, S. G.; Hitchcock, A. P.; Ade, H.; Smith, A. P.; Mitchell, G. E.; Priester, R. D.; Aneja, A.; Appel, G.; Wilkes, G.; Lidy, W. E. *Macromolecules* **2002**, *35*, 5873–5882.
53. Hook, F.; Voros, J.; Rodahl, M.; Kurrat, R.; Boni, P.; Ramsden, J. J.; Textor, M.; Spencer, N. D.; Tengvall, P.; Gold, J.; Kasemo, B. *Colloids Surf., B* **2002**, *24*, 155–170.
54. Rechendorff, K.; Hovgaard, M. B.; Foss, M.; Zhdanov, V. P.; Besenbacher, F. *Langmuir* **2006**, *22*, 10885–10888.
55. Weidner, T.; Ballav, N.; Siemeling, U.; Troegel, D.; Walter, T.; Tacke, R.; Castner, D. G.; Zharnikov, M. *J. Phys. Chem. C* **2009**, *113*, 19609–19614.
56. Diaz-Mochon, J. J.; Tourniaire, G.; Bradley, M. *Chem. Soc. Rev.* **2007**, *36*, 449–457.
57. Lahann, J.; Langer, R. *MRS Bull.* **2005**, *30*, 185–188.
58. Kingshott, P.; Griesser, H. J. *Curr. Opin. Solid State Mater. Sci.* **1999**, *4*, 403–412.
59. Chen, C. S.; Jang, X.; Whitesides, G. M. *MRS Bull.* **2005**, *30*, 194–201.
60. Bretagnol, F.; Valsesia, A.; Ceccone, G.; Colpo, P.; Gilland, D.; Ceriotti, L.; Hasiwa, M.; Rossi, F. *Plasma Proc. Polym.* **2006**, *3*, 443–455.
61. Sardella, E.; Favia, P.; Gristina, R.; Nardulli, R.; D'Agostino, R. *Plasma Processes Polym.* **2006**, *3*, 456–459.

62. Dewez, J. L.; Doren, A.; Schneider, Y.; Rouxhet, P. G. *Biomaterials* **1999**, *20*, 547–559.
63. Morra, M. *Biomacromolecules* **2005**, *6*, 1205–1223.
64. Pickard, C. M. In *Ubiquitin and biology of the cell*; Peters, J. M., Harris, J. R., Finley, D., Eds.; Kleuwer Academic Press: New York, 1998.
65. Hale, P.; Turgeon, S.; Horny, P.; Lewis, F.; Brack, N.; Van Riessen, G.; Pigram, P.; Mantovani, D. *Langmuir* **2008**, *24*, 7897–7905.
66. Chevallier, P.; Holvoet, S.; Turgeon, S.; Horny, P.; Pireaux, J. J.; Mantovani, D. *J. Appl. Polym. Sci.* **2010**, *118*, 3176–3186.
67. Kappen, P.; Hale, P. S.; Brack, N.; Prissanaroon, W.; Pigram, P. J. *Appl. Surf. Sci.* **2006**, *253*, 1473–1479.